STREAMLINE
This project has received funding from the European Union's Horizon 2020 research and innovation programme under grant agreement No 870313.

ID11 Materials Science: Diffraction and Imaging

Jonathan Wright
Haixing Fang
Wolfgang Ludwig
Pierre-Olivier Autran
James Ball
Pedro Damas-Resende
Zheheng Liu
Henri Gleyzolle
Eric Gagliardini
Emmanuel Papillon
Jose Maria Clement

Photo credit: S. Cande/ESRF

ID11 Materials Science beamline : upgraded 2006, nanofocus station since 2016

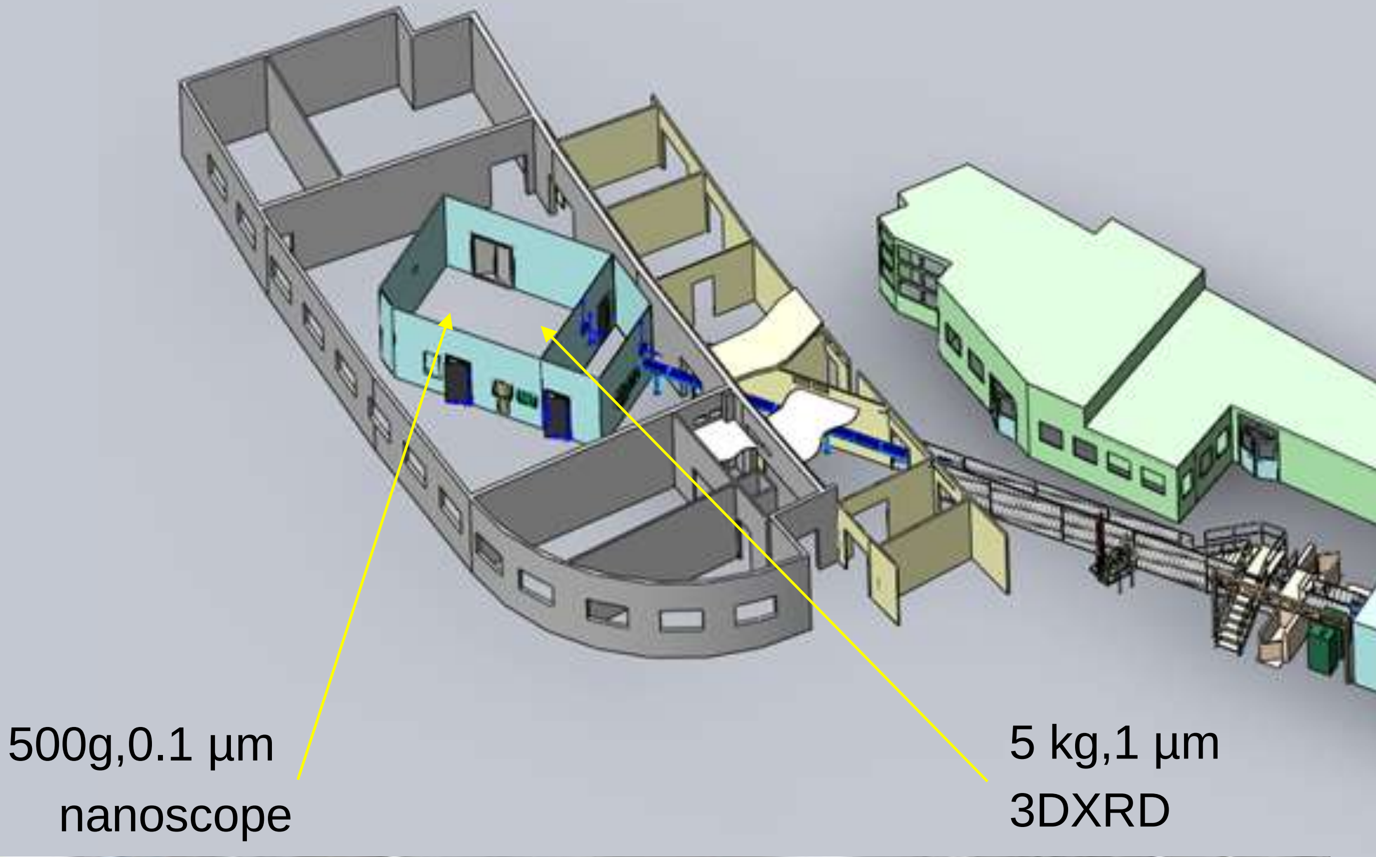

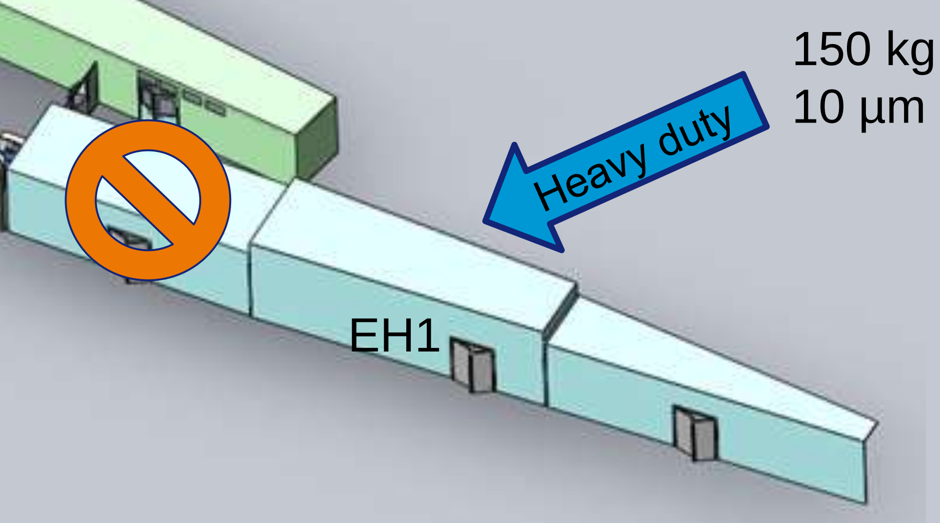

ESRF Upgrade Phase II : new source in 2019-2020 + new detectors

~40X more photons for ID11 optics

2 in-vacuum undulators
High power density at front end

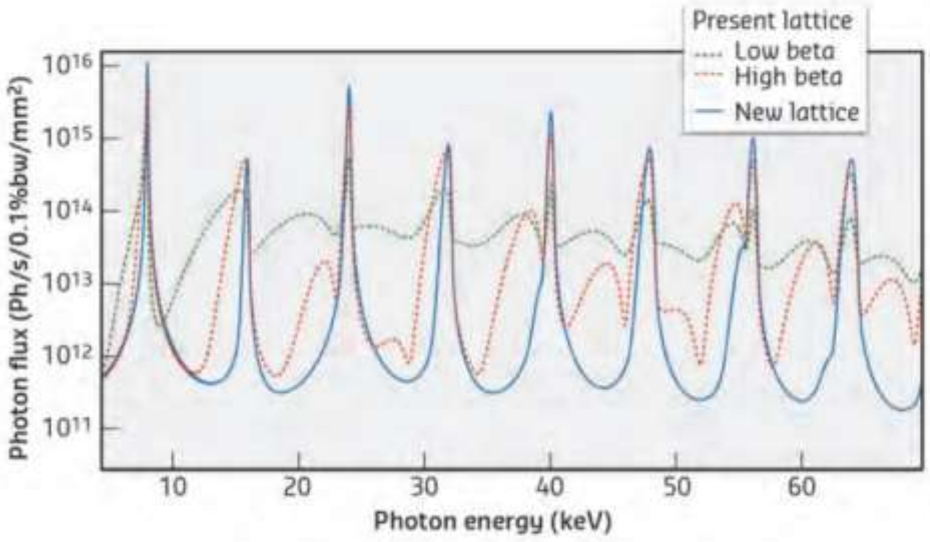

Eiger2 4M CdTe, 500 fps

2x Marana sCMOS (24 fps @16bit)

New Optique Peter Imaging Microscope

Flux is often sufficient

https://doi.org/10.1107/S160057752100669X

Beam heating from a fourth-generation synchrotron source

J. Synchrotron Rad. (2021). **28**, 1377–1385

Eleanor Lawrence Bright,* Carlotta Giacobbe and Jonathan P. Wright

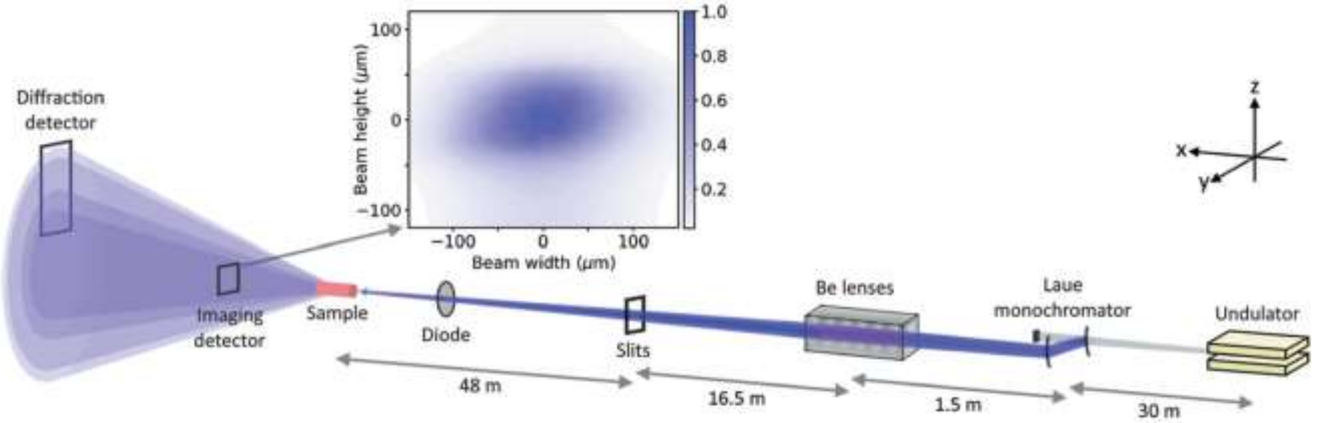

Figure 1
Schematic of the experimental set-up at the ID11 beamline, with a plot showing an image of the focused beam.

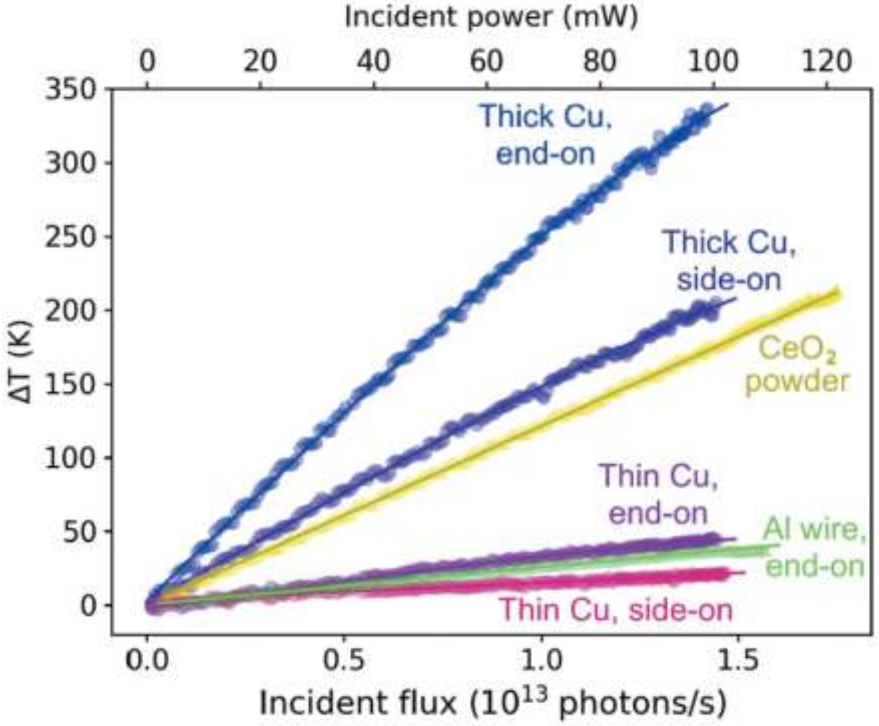

Figure 2
Change in temperature of samples as a function of incident flux, with 0.19 mm-thick and 0.025 mm-thin Cu wire aligned end-on or side-on to the beam, a 0.5 mm capillary of CeO_2, and 0.5 mm Al wire.

Recrystallisation of copper due to beam heating. Lawrence-Bright *et-al*

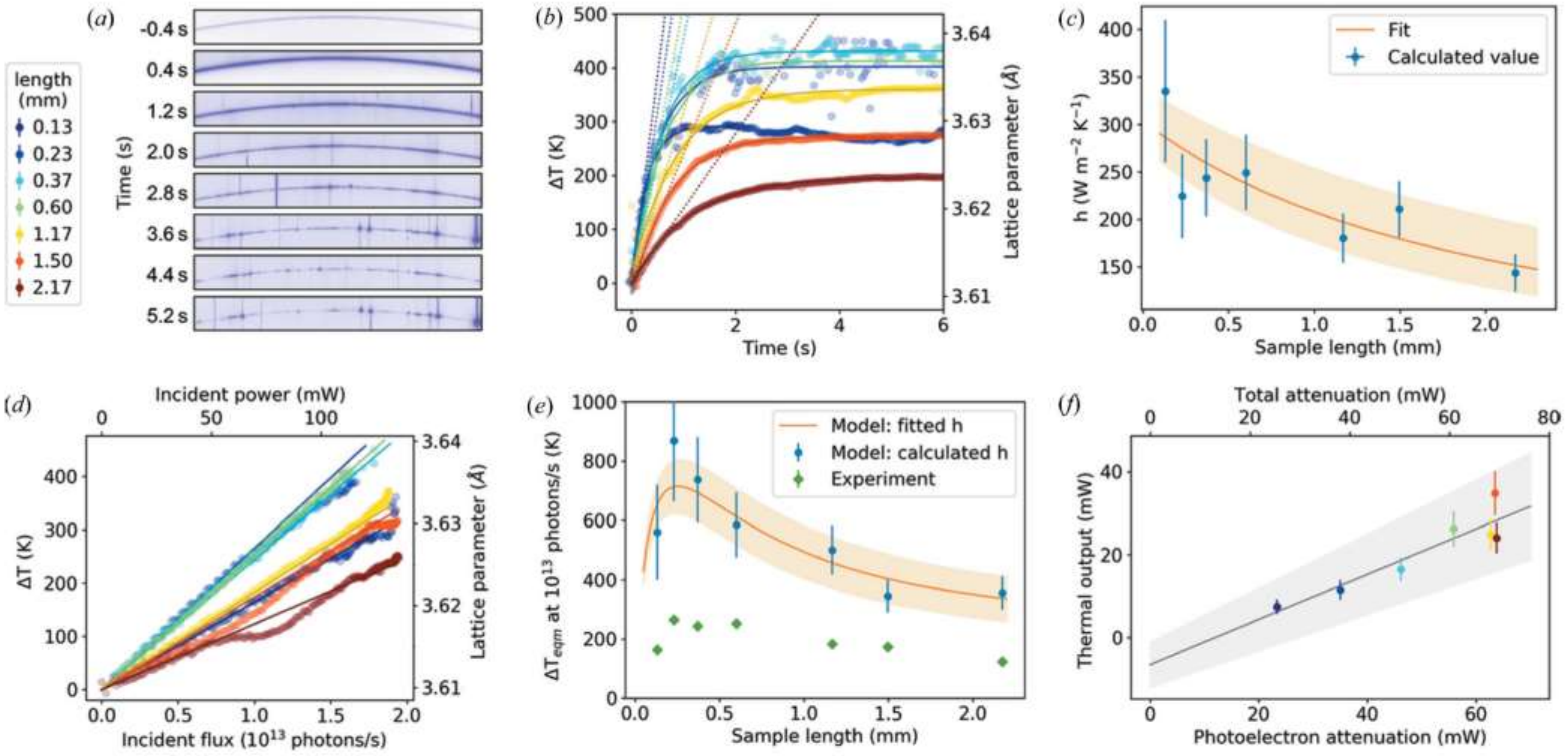

Figure 5

Results for 0.19 mm-diameter Cu wire samples of varying lengths (see legend), with (*a*) images of the (222) reflection as a function of time after insertion of focusing lenses into the beam from a 0.86 mm-length sample, (*b*) the change in temperature as a function of time after insertion of focusing lenses, (*c*) calculated *h* values as a function of length, (*d*) change in temperature as a function of incident flux, (*e*) measured and modelled change in temperature at 10^{13} photons s^{-1}, and (*f*) calculated thermal output at 10^{13} photons s^{-1} against X-ray beam attenuation.

Diffraction Experiments : *adapted to the sample*

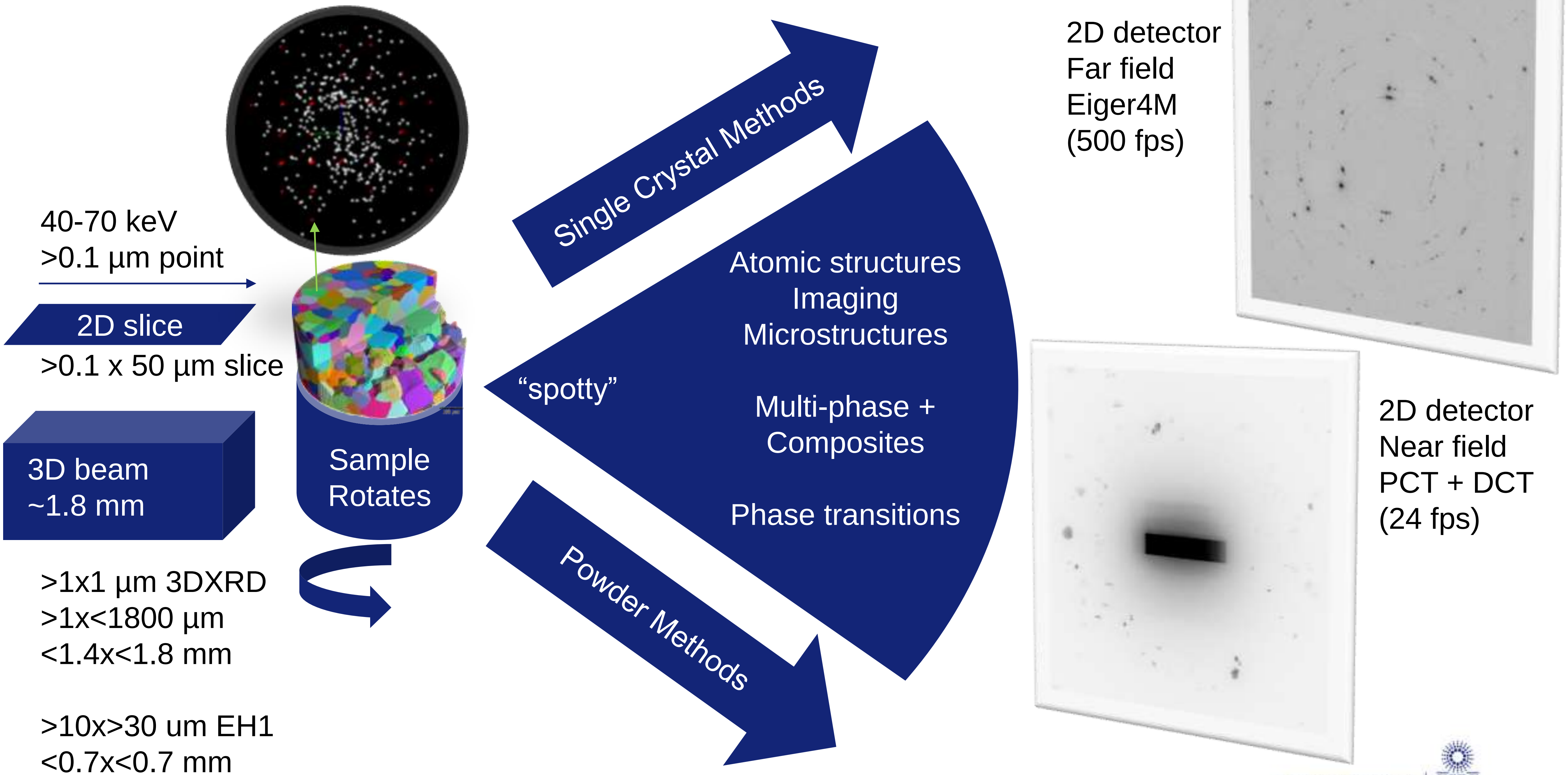

Single crystal diffraction, nanoscope station (2023 pubs)

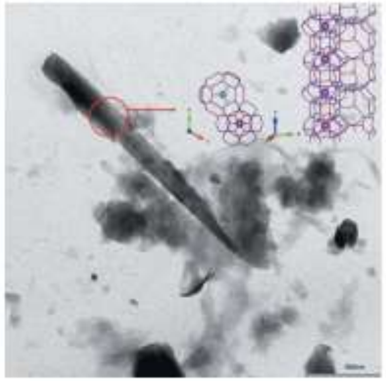

The crystal structure of the killer fibre erionite from Tuzköy (Cappadocia, Turkey)

Carlotta Giacobbe,[a*] Anna Moliterni,[b*] Dario Di Giuseppe,[c] Daniele Malferrari,[c] Jonathan P. Wright,[a] Michele Mattioli,[d] Simona Raneri,[e] Cinzia Giannini,[b] Laura Fornasini,[e] Enrico Mugnaioli,[f] Paolo Ballirano[g] and Alessandro F. Gualtieri[c]

IUCrJ (2023). 10, 397–410

Chemistry
A European Journal
Chemistry Europe
European Chemical Societies Publishing

Research Article · Open Access

Modular Principle for Complex Disordered Tetrahedral Frameworks in Quenched High-Pressure Phases of Phosphorus Oxide Nitrides

Daniel Günther, Dr. Dominik Baumann, Prof. Dr. Wolfgang Schnick, Prof. Dr. Oliver Oeckler

What happens when you're under pressure: The tetrahedral frameworks of $P_{40}O_{21}N_{46}$ and $P_{74}O_{69}N_{84}$ correspond to quenched high-pressure phases and can be described as different arrangements of the same modular building units. The crystal structures were determined from fragments intergrown with the structurally related compound $H_3P_8O_8N_9$.

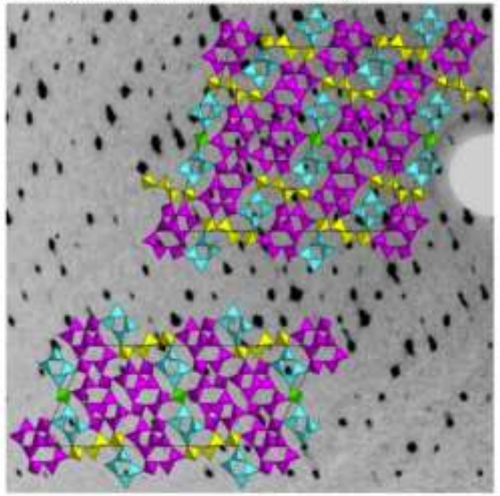

Closing the knowledge gap on the composition of the asbestos bodies

F. Bardelli · C. Giacobbe · P. Ballirano · V. Borelli ·
F. Di Benedetto · G. Montegrossi · D. Bellis ·
A. Pacella

Environ Geochem Health (2023) 45:5039–5051
https://doi.org/10.1007/s10653-023-01557-0

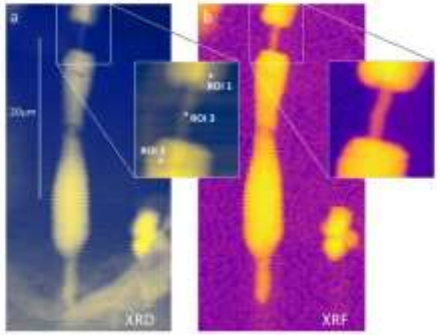

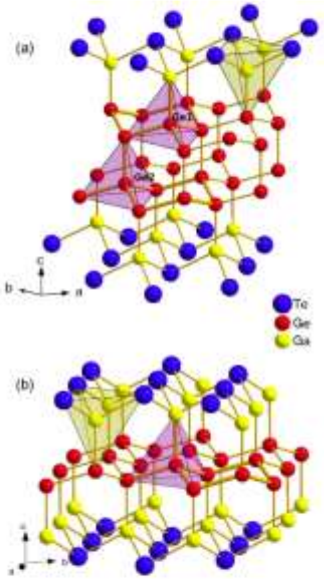

Figure 1. One layer of the crystal structures of $GaGe_2Te$ (a) and GaGeTe (b); the coordination polyhedra around the Ge and Ga atoms as well as some chair-like six-membered rings are highlighted.

The structure of the crystalline lithium oxonitridophosphate [illegible] contains three different anions, namely [illegible], [illegible], and O^{2-}. It was comprehensively investigated by single-crystal and powder X-ray diffraction, neutron powder diffraction, NMR spectroscopy and elemental analysis. A total ionic conductivity of [illegible], which is similar to that of amorphous a-LiPON was determined with impedance spectroscopy.

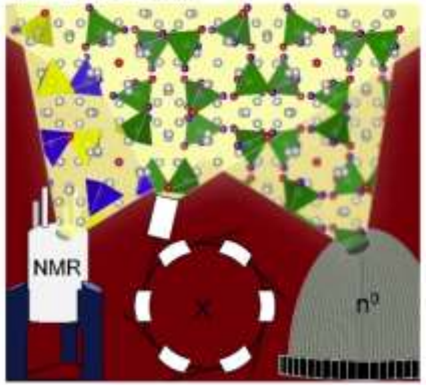

Chemistry
A European Journal
Chemistry Europe
European Chemical Societies Publishing

Research Article · Open Access

Comprehensive Investigation of Anion Species in Crystalline Li⁺ ion Conductor $Li_{27-x}[P_4O_{7+x}N_{9-x}]O_3$ ($x \approx 1.9(3)$)

Stefanie Schneider, Dr. Eva-Maria Wendinger, Dr. Volodymyr Baran, Dr. Anna-Katharina Hatz, Prof. Dr. Bettina V. Lotsch, Dr. Markus Nentwig, Prof. Dr. Oliver Oeckler, Dr. Thomas Bräuniger, Prof. Dr. Wolfgang Schnick ... See fewer authors

DOI: 10.1002/zaac.202300107

Layered $GaGe_2Te$: structure and chemical bonding

Tobias Juhlke,[a] Simon Steinberg,[b] Lennart Staab,[a] Eleanor Lawrence Bright,[c] and Oliver Oeckler*[a]

High pressure : 2D diffraction map, select crystals, rotation scan for 3D single crystal structure

VIP **Polynitrides** *Very Important Paper*

How to cite: *Angew. Chem. Int. Ed.* **2022**, *61*, e202207469
International Edition: doi.org/10.1002/anie.202207469
German Edition: doi.org/10.1002/ange.202207469

Anionic N_{18} Macrocycles and a Polynitrogen Double Helix in Novel Yttrium Polynitrides YN_6 and Y_2N_{11} at 100 GPa

Andrey Aslandukov, Florian Trybel, Alena Aslandukova, Dominique Laniel, Timofey Fedotenko, Saiana Khandarkhaeva, Georgios Aprilis, Carlotta Giacobbe, Eleanor Lawrence Bright, Igor A. Abrikosov, Leonid Dubrovinsky, and Natalia Dubrovinskaia*

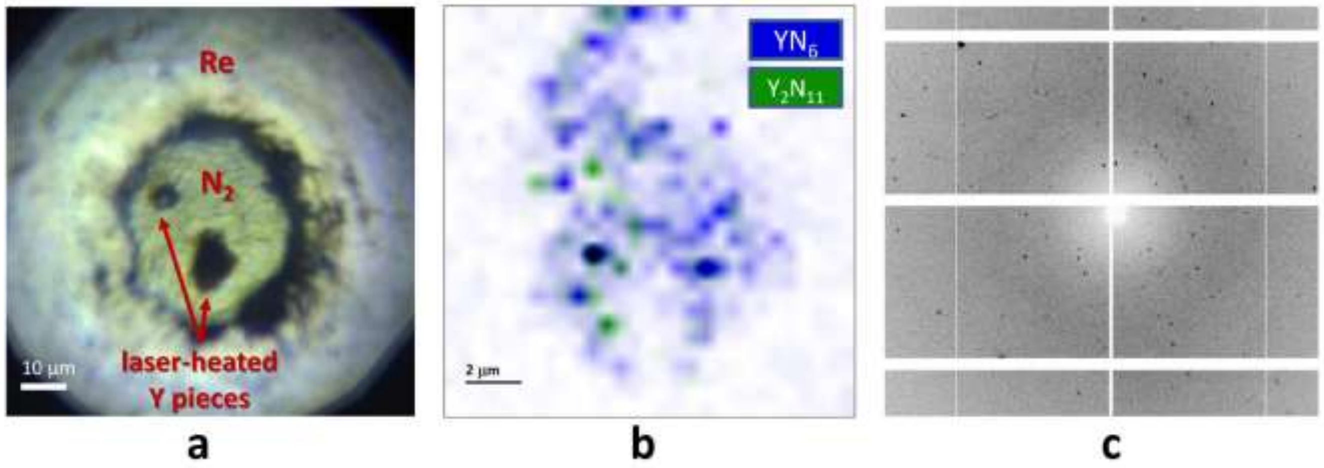

Figure 1. Experimental details. a) Microphotograph of the sample chamber. b) 2D X-ray diffraction map showing the distribution of the two yttrium nitrides phases within the heated sample. The color intensity is proportional to the intensity of the following reflections: the (2 0 0), (0 2 0), and (1 1 -2) of YN_6 for the blue regions; the (1 0 1), (2 -1 0), and (2 -1 4) of Y_2N_{11} for the green regions. c) Example of an X-ray diffraction pattern collected from the laser-heated sample at 100 GPa.

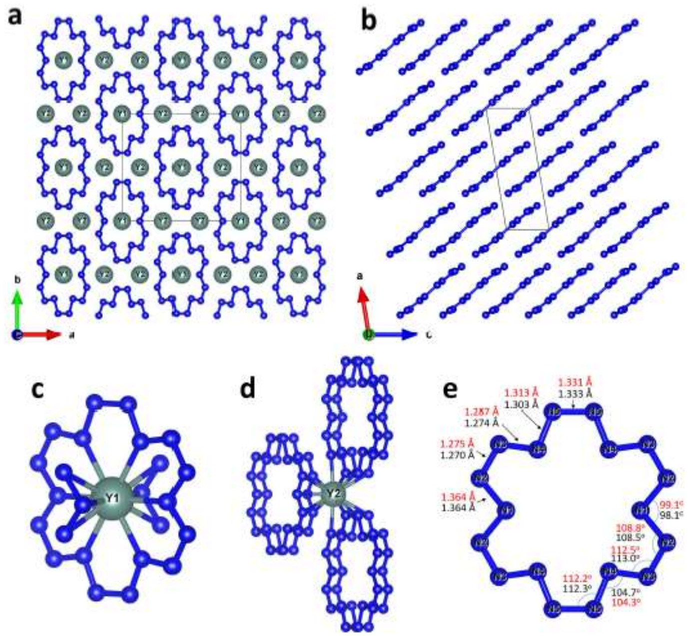

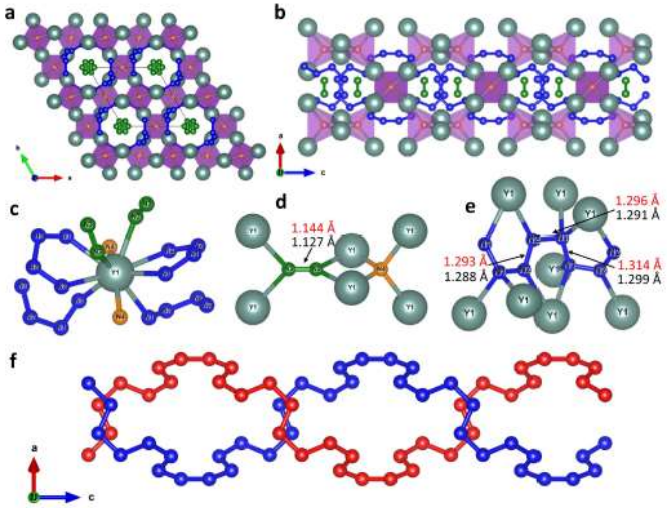

High pressure diamond anvil crystallography (pubs 2023)

2D XRD map + select xtal + rotation scan

nature chemistry

Article

https://doi.org/10.1038/s41557-023-01148-7

Aromatic hexazine $[N_6]^{4-}$ anion featured in the complex structure of the high-pressure potassium nitrogen compound K_9N_{56}

b

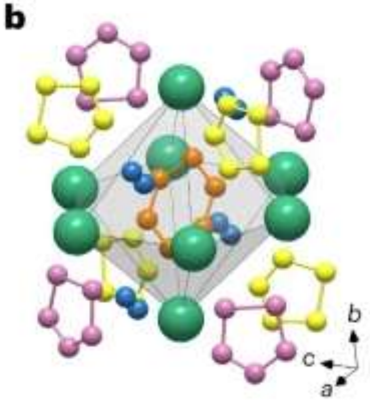

Dominique Laniel[1,2], Florian Trybel[3], Yuqing Yin[1,4], Timofey Fedotenko[1], Saiana Khandarkhaeva[5], Andrey Aslandukov[1], Georgios Aprilis[6], Alexei I. Abrikosov[7], Talha Bin Masood[7], Carlotta Giacobbe[6], Eleanor Lawrence Bright[6], Konstantin Glazyrin[8], Michael Hanfland[6], Jonathan Wright[6], Ingrid Hotz[7], Igor A. Abrikosov[3], Leonid Dubrovinsky[4] & Natalia Dubrovinskaia[1,3]

nature communications

Article

https://doi.org/10.1038/s41467-023-41968-2

Structure determination of ζ-N_2 from single-crystal X-ray diffraction and theoretical suggestion for the formation of amorphous nitrogen

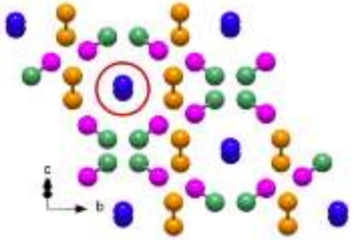

Dominique Laniel[1], Florian Trybel[2], Andrey Aslandukov[3,4], James Spender[1], Umbertoluca Ranieri[1], Timofey Fedotenko[5], Konstantin Glazyrin[5], Eleanor Lawrence Bright[6], Stella Chariton[7], Vitali B. Prakapenka[7], Igor A. Abrikosov[2], Leonid Dubrovinsky[4] & Natalia Dubrovinskaia[2,3]

JACS Au

pubs.acs.org/jacsau Article

Unraveling the Bonding Complexity of Polyhalogen Anions: High-Pressure Synthesis of Unpredicted Sodium Chlorides Na_2Cl_3 and Na_4Cl_5 and Bromide Na_4Br_5

Yuqing Yin,* Alena Aslandukova, Nityasagar Jena, Florian Trybel, Igor A. Abrikosov, Bjoern Winkler, Saiana Khandarkhaeva, Timofey Fedotenko, Elena Bykova, Dominique Laniel, Maxim Bykov, Andrey Aslandukov, Fariia I. Akbar, Konstantin Glazyrin, Gaston Garbarino, Carlotta Giacobbe, Eleanor L. Bright, Zhitai Jia, Leonid Dubrovinsky, and Natalia Dubrovinskaia

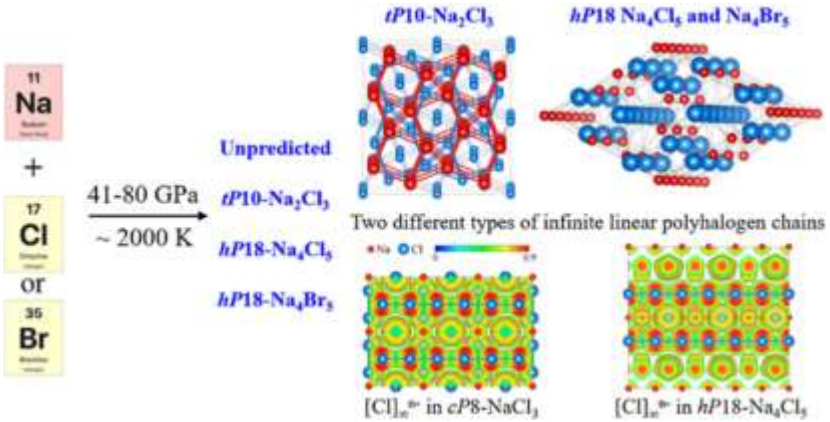

Acta Cryst. (2023). E79, 923-925
https://doi.org/10.1107/S2056989023008058

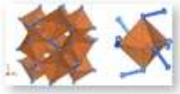

Synthesis and crystal structure of silicon pernitride SiN_2 at 140 GPa

P. L. Jurzick, G. Krach, L. Brüning, W. Schnick and M. Bykov

Near-field and far-field detectors : suite of 3DXRD methods

Pixels smaller than crystals

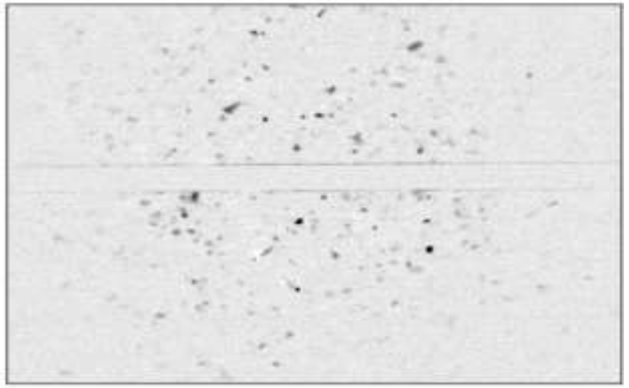

Near Field HEDM
(usually 2D, line focus slices)

1D Point focus
2D Line focus
3D Beam

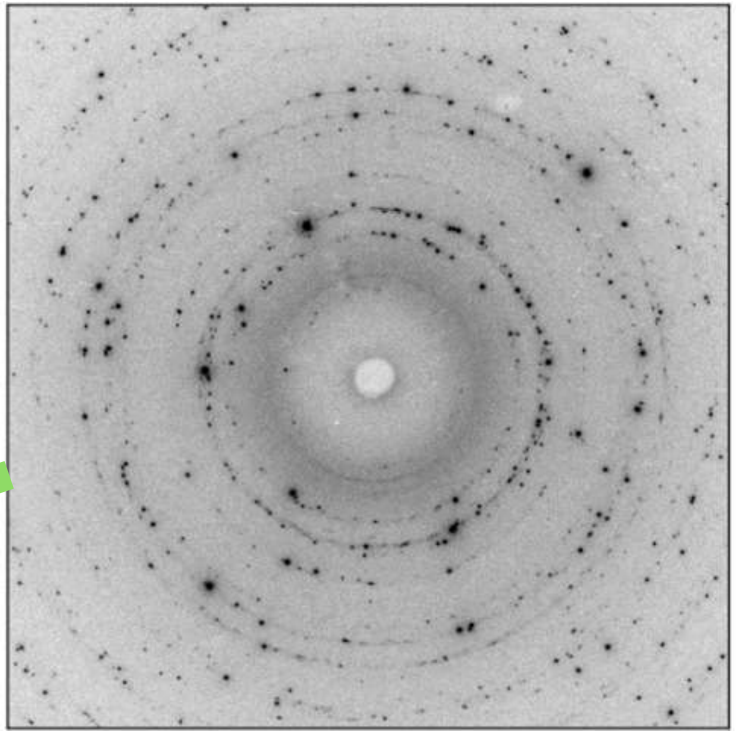

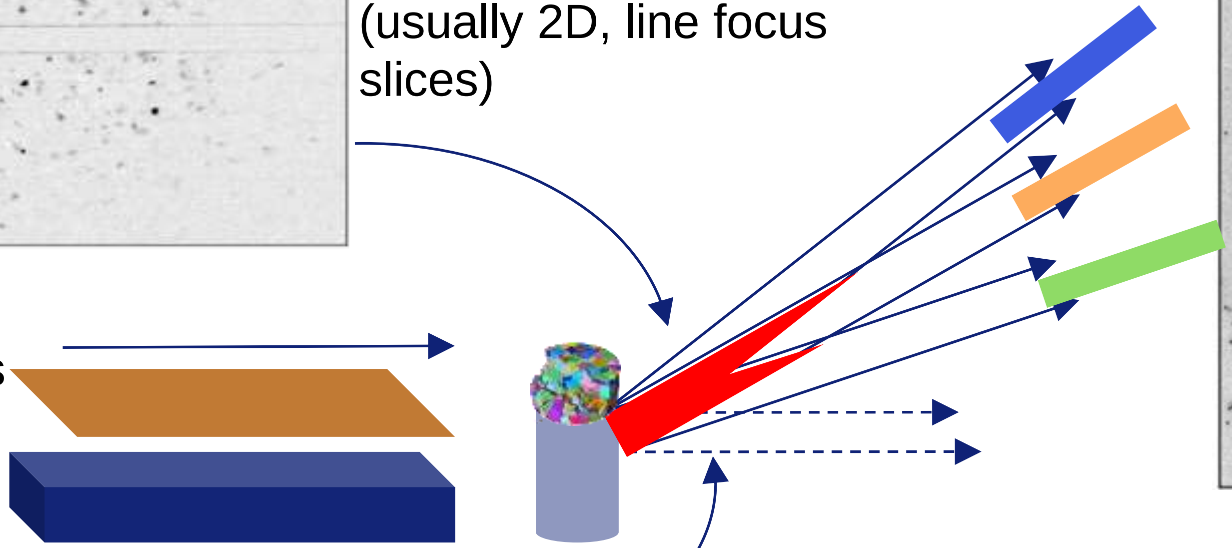

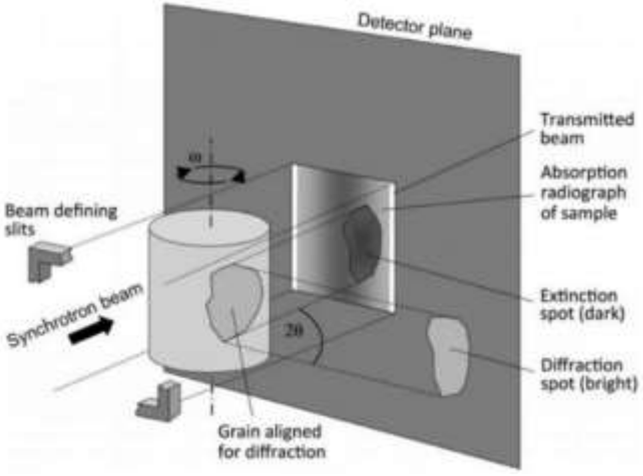

DCT =
Diffraction
Contrast
Tomography
(3D)

Pixels larger than crystals

- Single crystal XRD
- Far-Field HEDM
- “Box Beam”
- “point scanning”

Calcium Sulfate hemihydrate–gypsum transformation

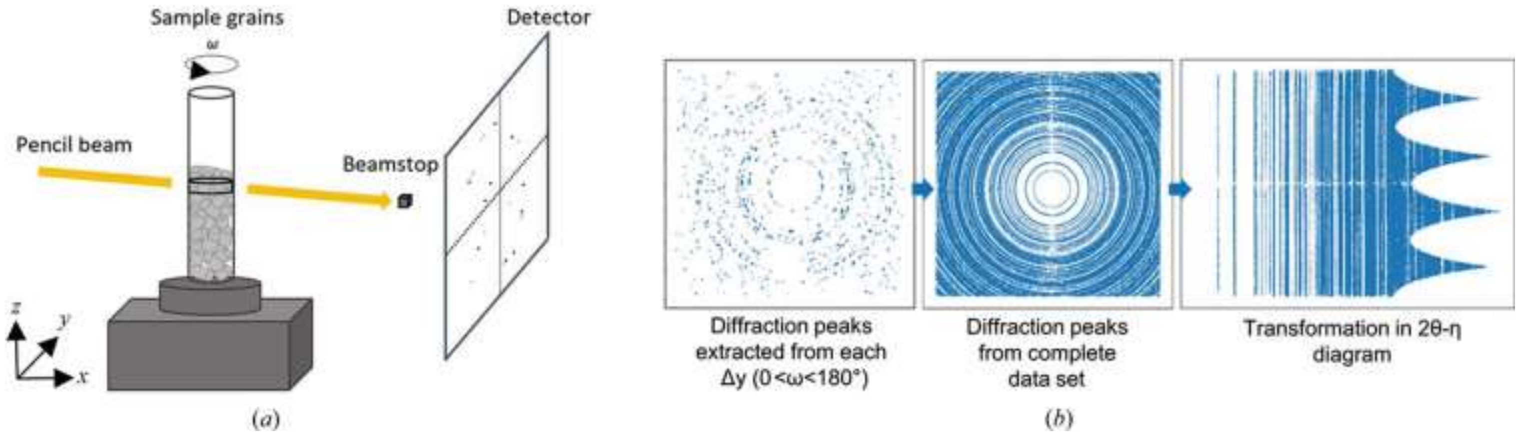

s3DXRD

PCT

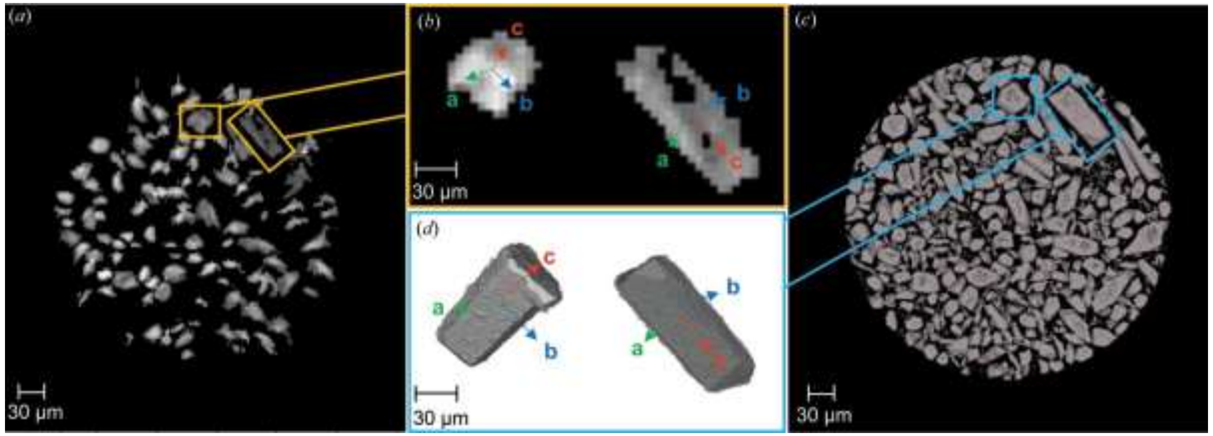

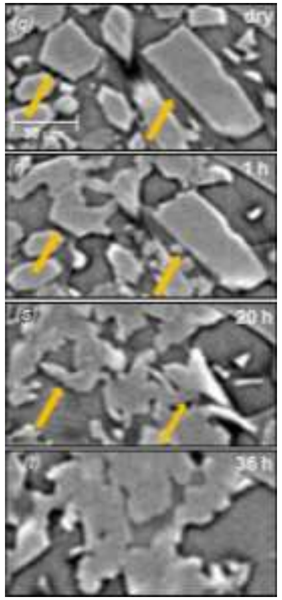

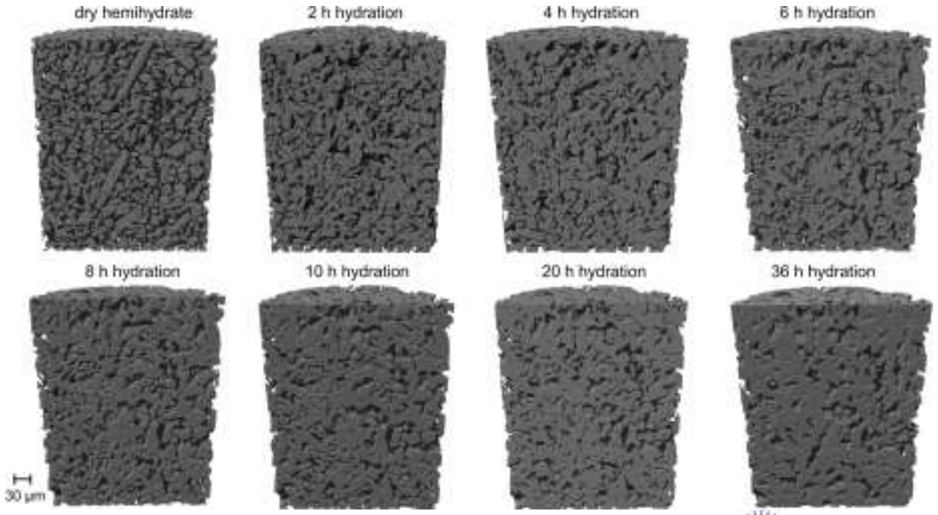

J. Appl. Cryst, (2023) **56,** 660.

Michela La Bella,[a,b]* Rogier Besselink,[b] Jonathan P. Wright,[a] Alexander E. S. Van Driessche,[b,c] Alejandro Fernandez-Martinez[b] and Carlotta Giacobbe[a]

Shape Memory Alloy

Super-elastic deformation in Cu-Al-Be alloy:

- **Microstructure from DCT**
- **Full strain tensor via 3DXRD**
- **FEM simulation model**

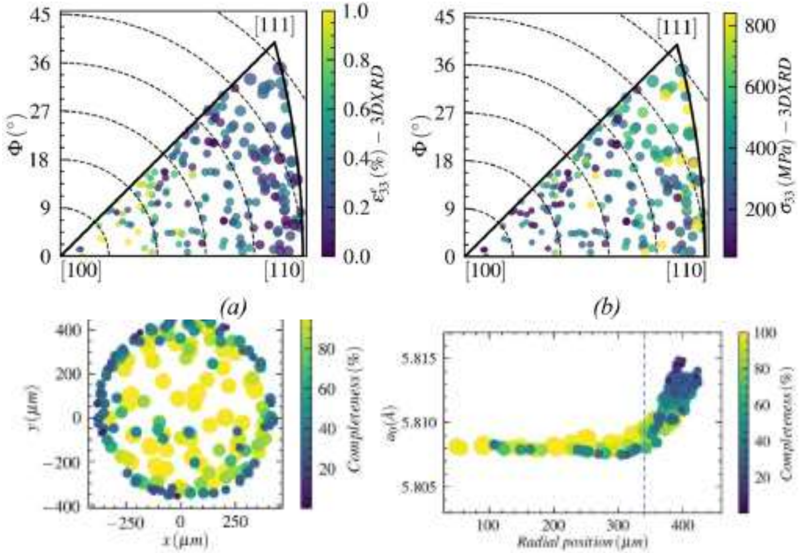

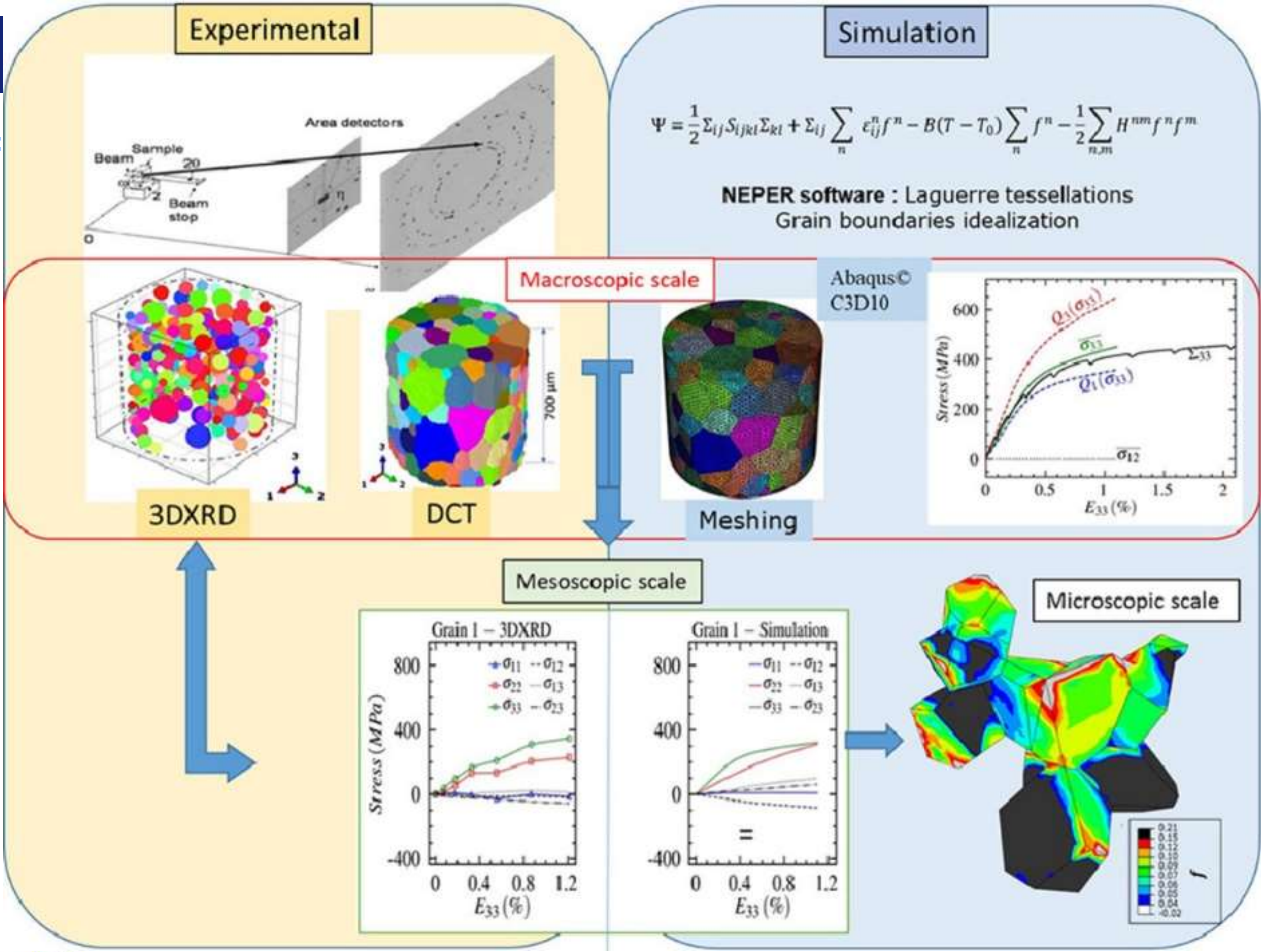

Acta Materialia 235 (2022) 118107

Multi-scale *in situ* mechanical investigation of the superelastic behavior of a Cu–Al–Be polycrystalline shape memory alloy

Y. El Hachi[a], S. Berveiller[a,*], B. Piotrowski[a], J. Wright[b], W. Ludwig[c], B. Malard[d]

Topo Tomography

Observation of bulk plasticity in a polycrystalline titanium alloy by diffraction contrast tomography and topotomography

J.C. Stinville [a], W. Ludwig [b c], P.G. Callahan [d], M.P. Echlin [e], V. Valle [f], T.M. Pollock [e], H. Proudhon [g]

Materials Characterization
Volume 188, June 2022, 111891

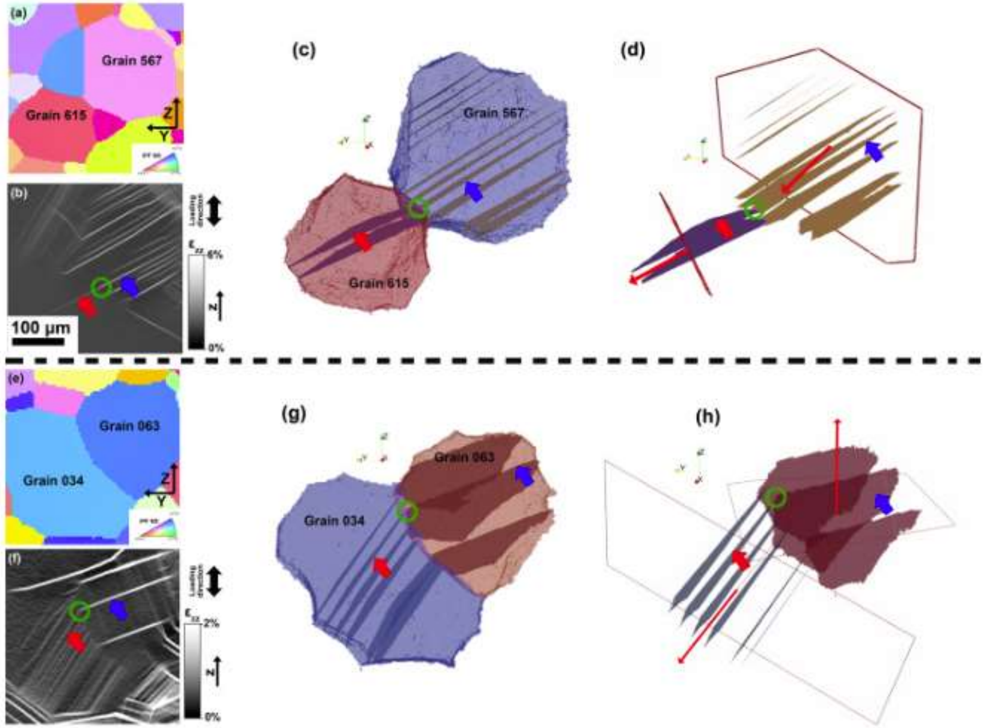

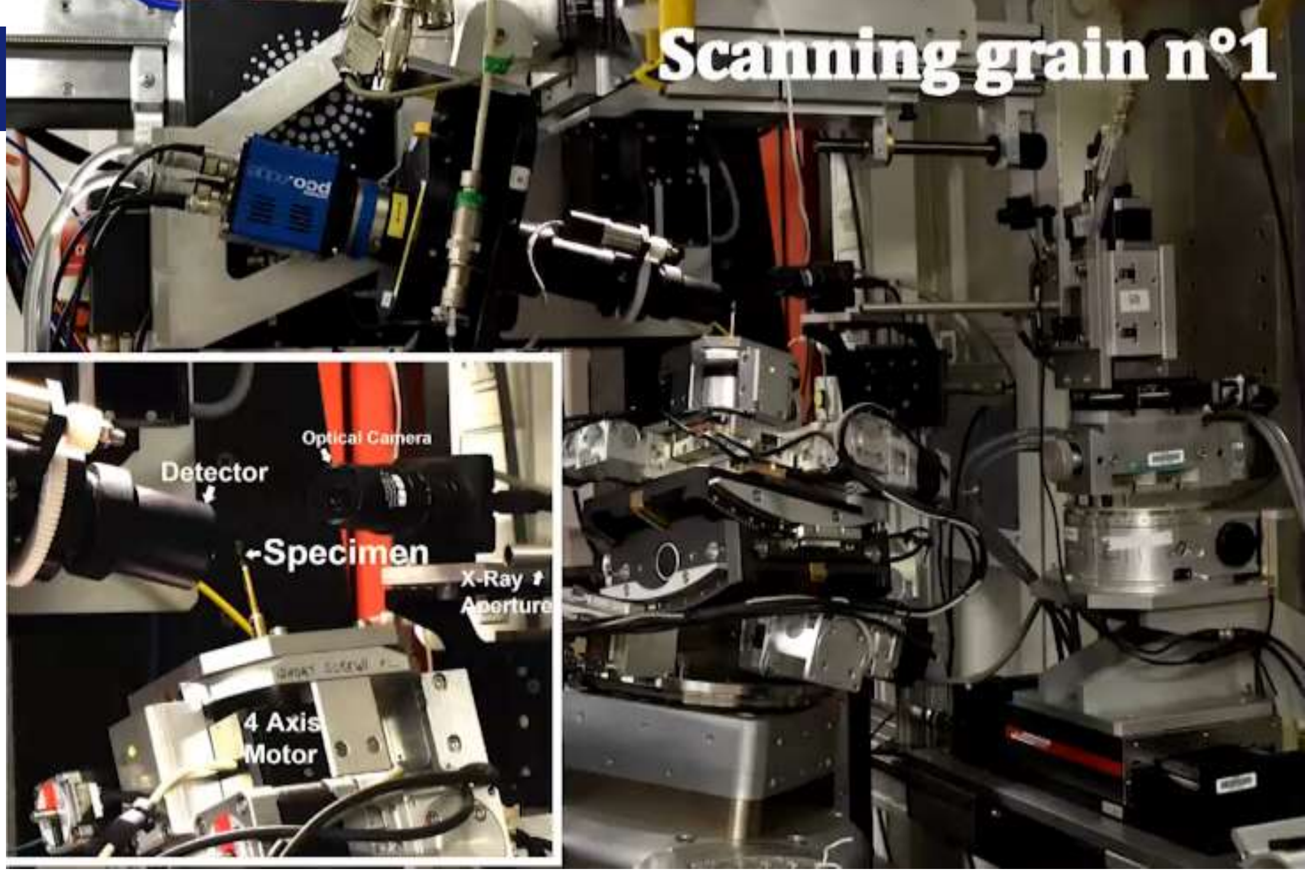

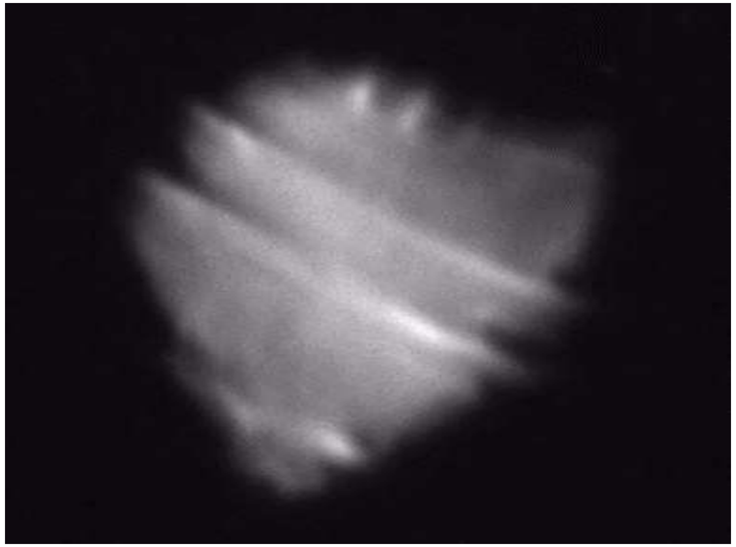

New control system. Macros developed to drive these scans (Wolfgang Ludwig, Henry Proudhon, LTP)

The European Synchrotron | ESRF

Inverse problems & reconstruction methods

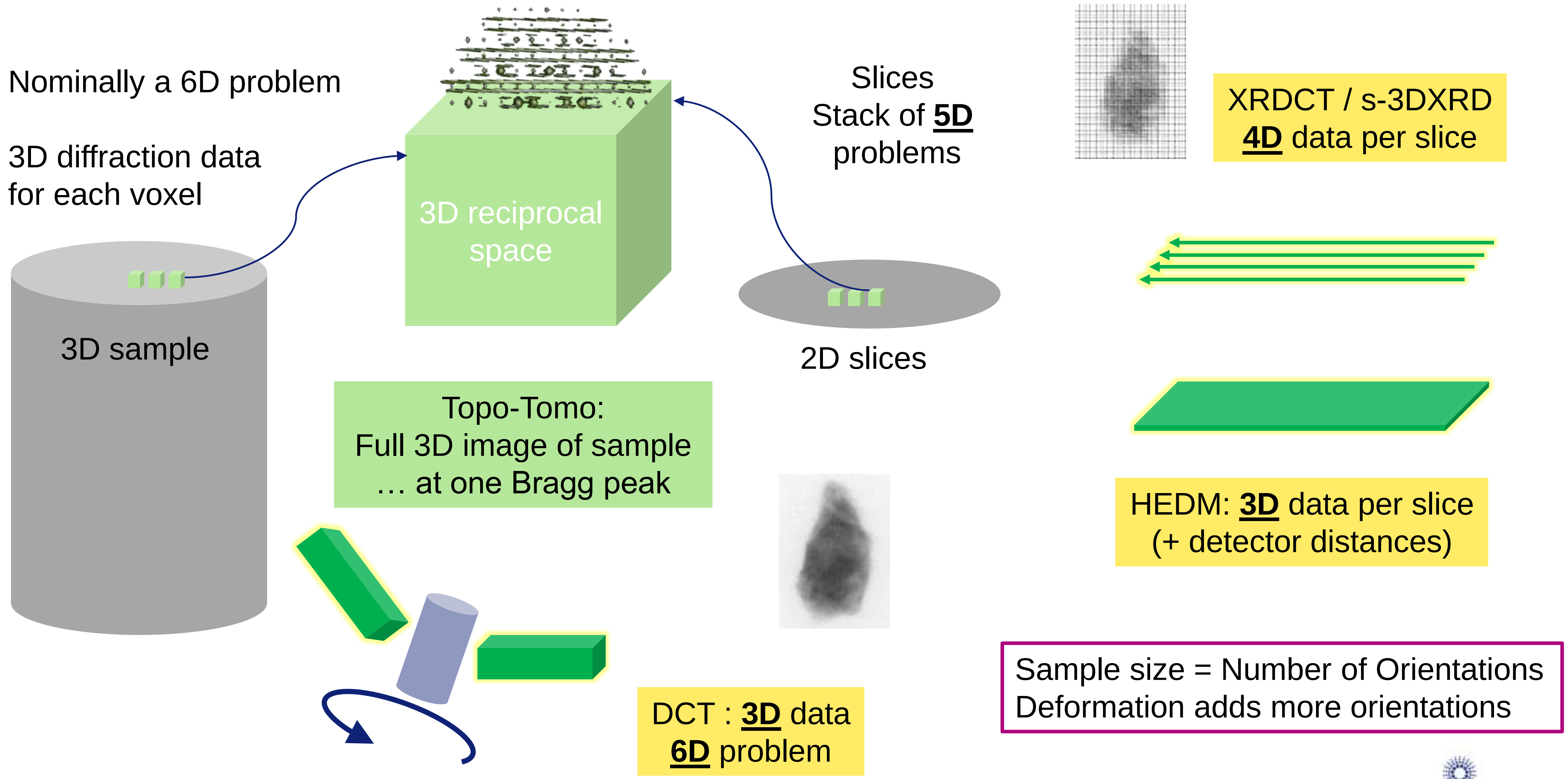

Imaging Via Diffraction : scanning method for glasses

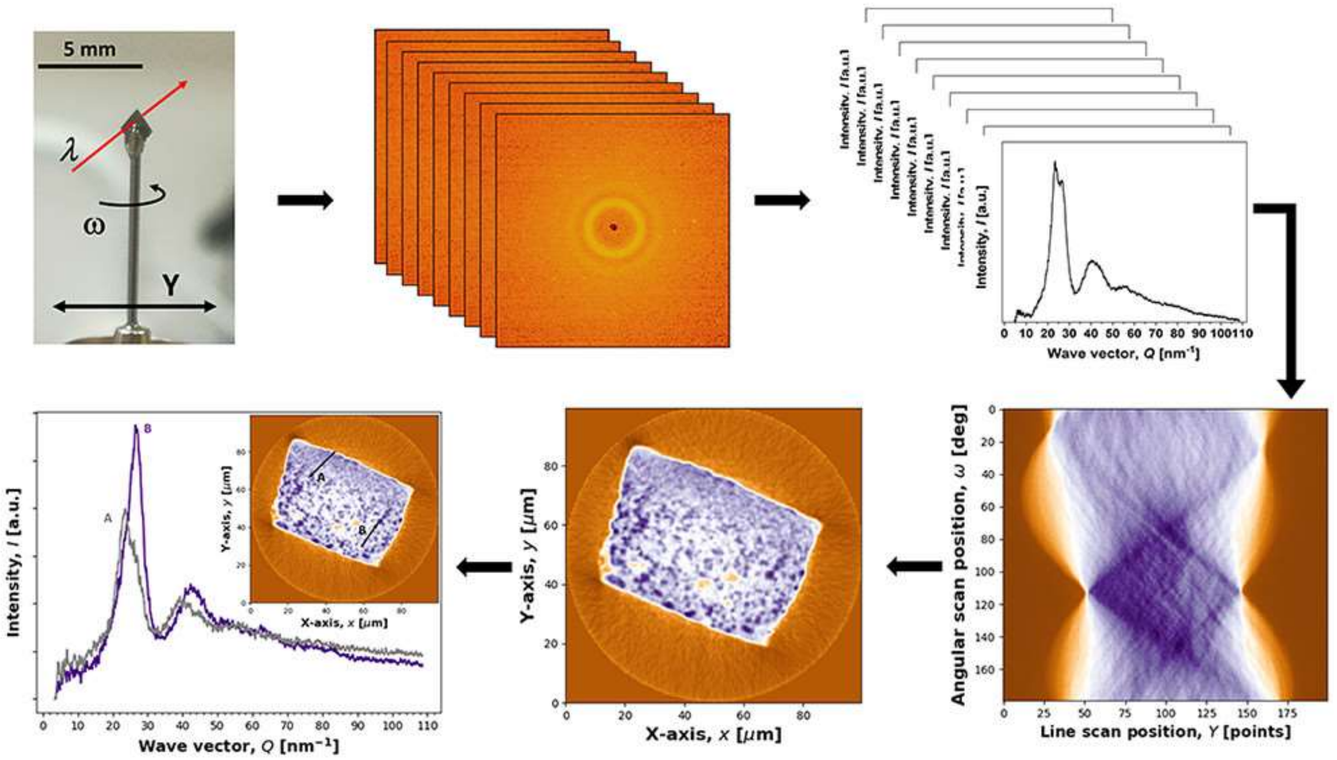

- **Amorphous,nanocrystalline**
- **Smooth S(Q), 1D function**
- **Radially symmetric**
- **Average 2D image -> 1D S(Q)**
- **iradon for each S(Q) pixel value**

ACSNANO

www.acsnano.org

X-ray Diffraction Computed Nanotomography Applied to Solve the Structure of Hierarchically Phase-Separated Metallic Glass

Mihai Stoica,* Baran Sarac, Florian Spieckermann, Jonathan Wright, Christoph Gammer, Junhee Han, Petre F. Gostin, Jürgen Eckert, and Jörg F. Löffler

Cite This: ACS Nano 2021, 15, 2386–2398   Read Online

XRDCT in bulk metallic glasses

Strain fields as local probe for X-ray diffraction tomography: Non-destructive reconstruction of shear band paths in metallic glasses

Sergio Scudino [a,*], Junhee Han [b], Rub Nawaz Shahid [a,1], Dina Bieberstein [a],
Thomas Gemming [a], Jon Wright [c]

S. Scudino, J. Han, R.N. Shahid et al. Journal of Alloys and Compounds 958 (2023) 17048

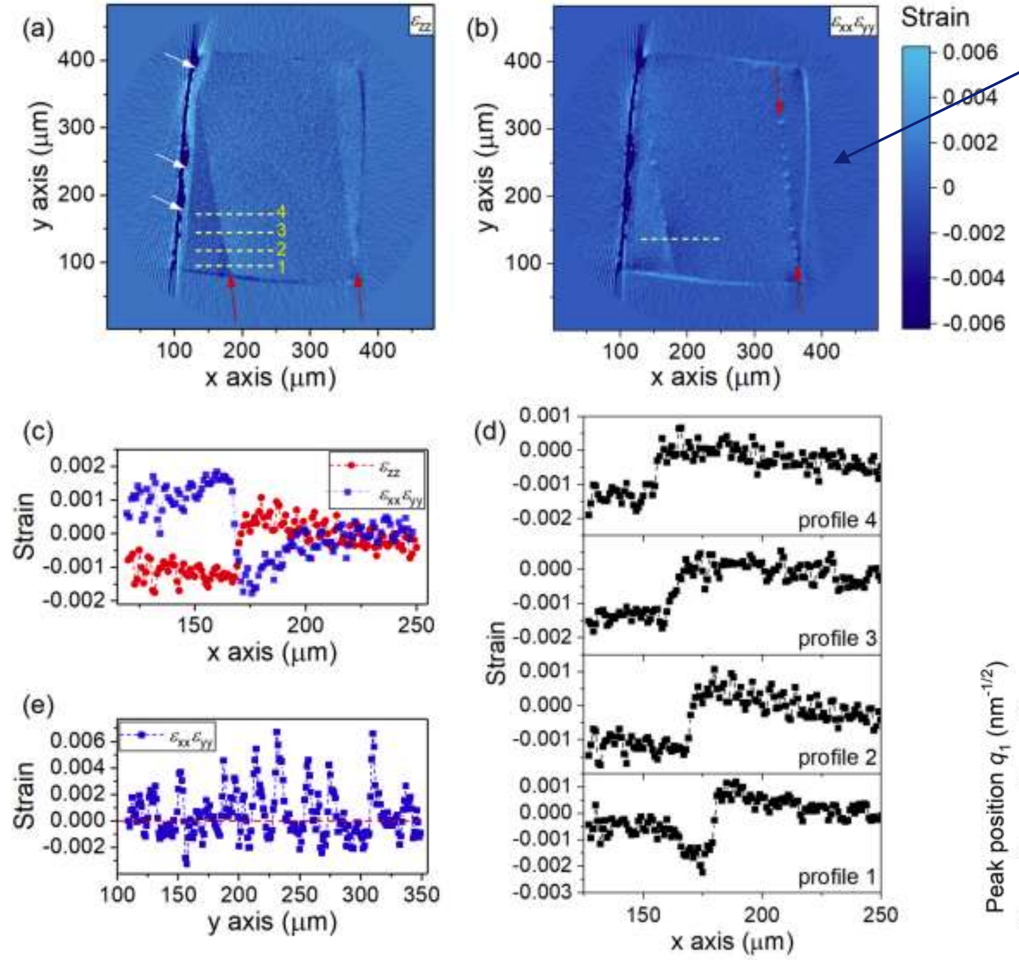

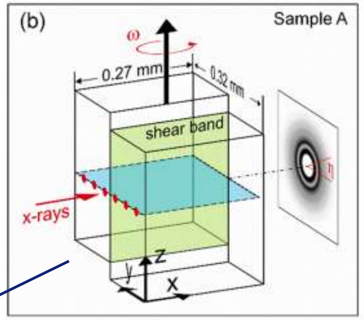

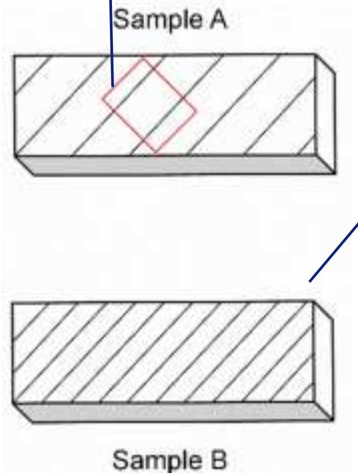

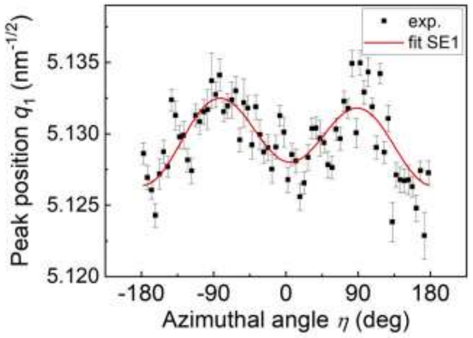

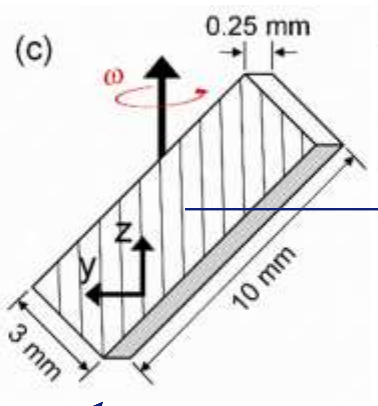

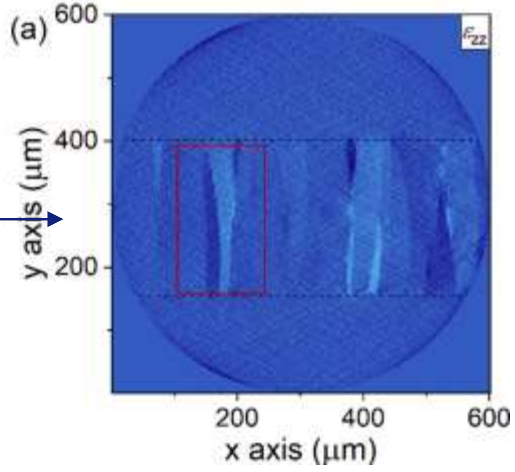

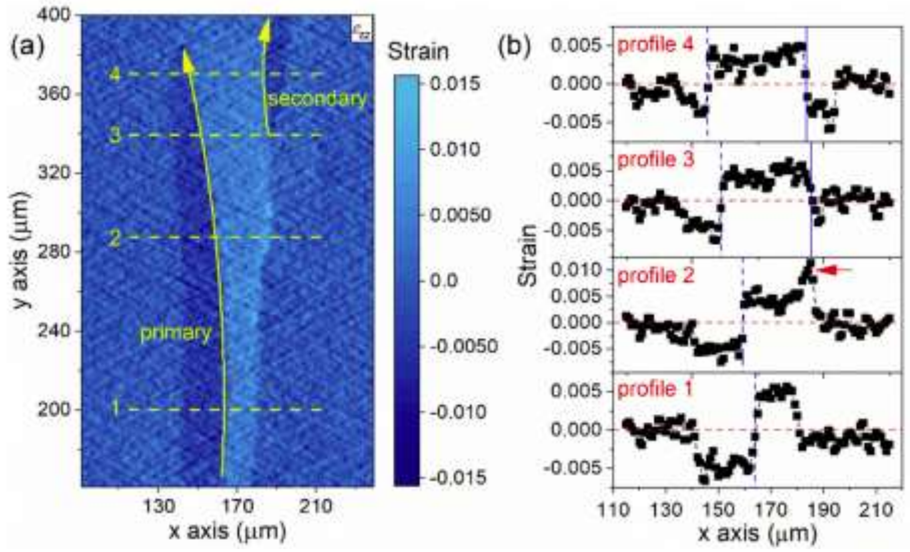

The European Synchrotron | ESRF

Strain tensor reconstruction

Scanning 3DXRD Measurement of Grain Growth, Stress, and Formation of Cu_6Sn_5 around a Tin Whisker during Heat Treatment

Johan Hektor [1,*], Stephen A. Hall [1,*], N. Axel Henningsson [1], Jonas Engqvist [1], Matti Ristinmaa [1], Filip Lenrick [2] and Jonathan P. Wright [3]

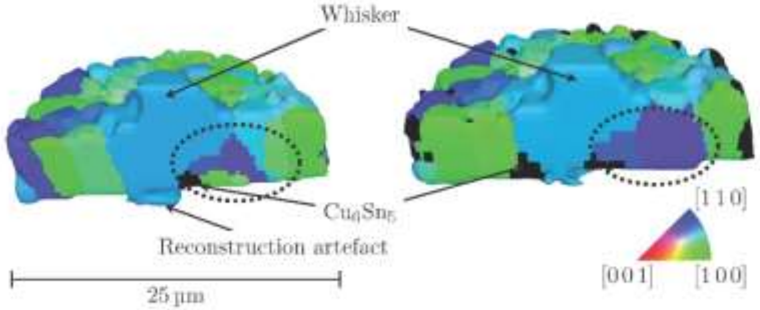

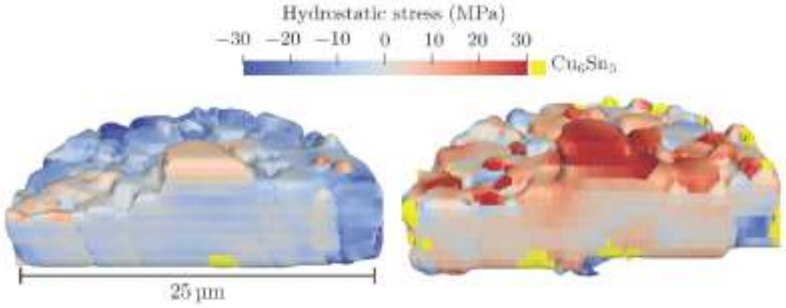

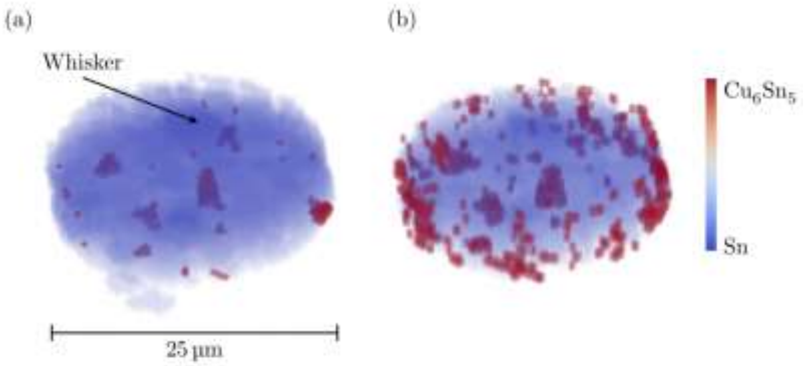

Figure 10. 3D map showing the location of Cu_6Sn_5 grains (red) in the Sn coating (blue): (**a**) before heat treatment; and (**b**) after heat treatment of 150 °C for three hours.

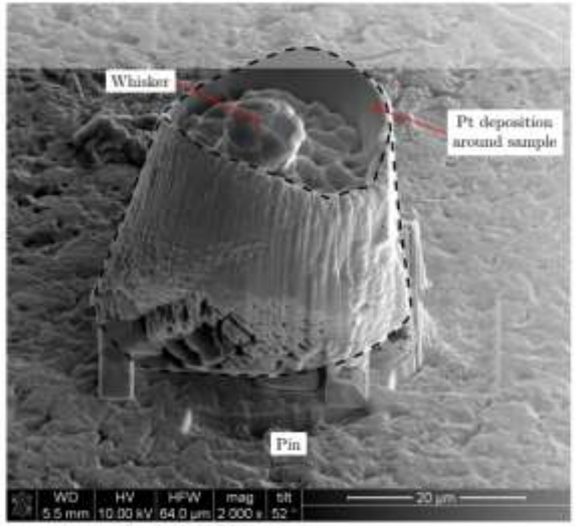

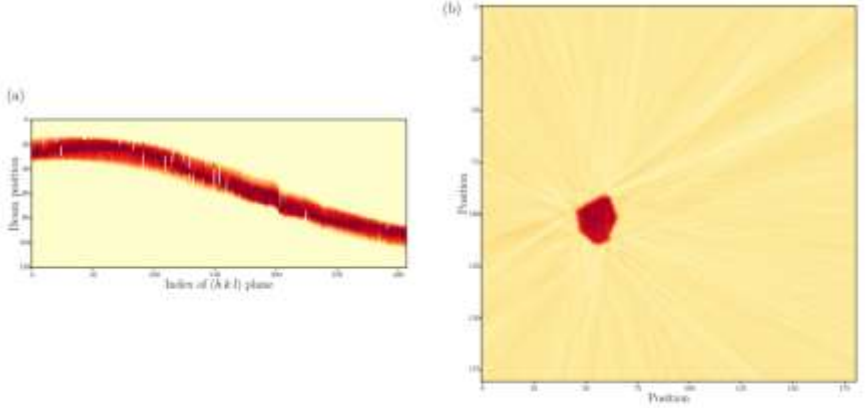

Figure 3. (**a**) Sinogram of one tin grain: The sinogram shows the sum of the intensities of all diffraction peaks belonging to the specific grain as a function of the diffracting lattice planes and the beam coordinate, y. The rows of the sinogram are normalised by the maximum intensity at each beam position. (**b**) Grain shape and position for one grain reconstructed by the inverse Radon transform of the sinogram.

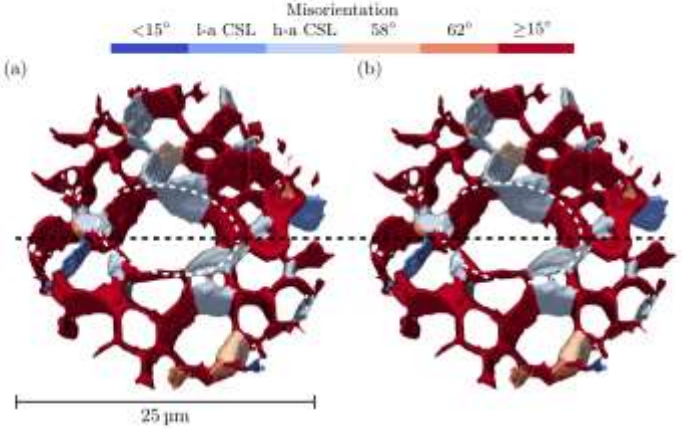

Figure 8. 3D renderings of the grain boundary network before and after heat treatment. The grain boundaries are coloured based on their misorientation angle. Blue and light blue represent low-angle CSL (l-a CSL) and high-angle CSL (h-a CSL) boundaries, respectively. The dashed ellipses indicate the location of the whisker. The dashed black line indicates where the volume in Figure 4 is sliced: (**a**) before heat treatment; and (**b**) after heat treatment.

Materials **2019**, *12*, 446; doi:10.3390/ma12030446

Strain reconstruction : Type II + III strain fields

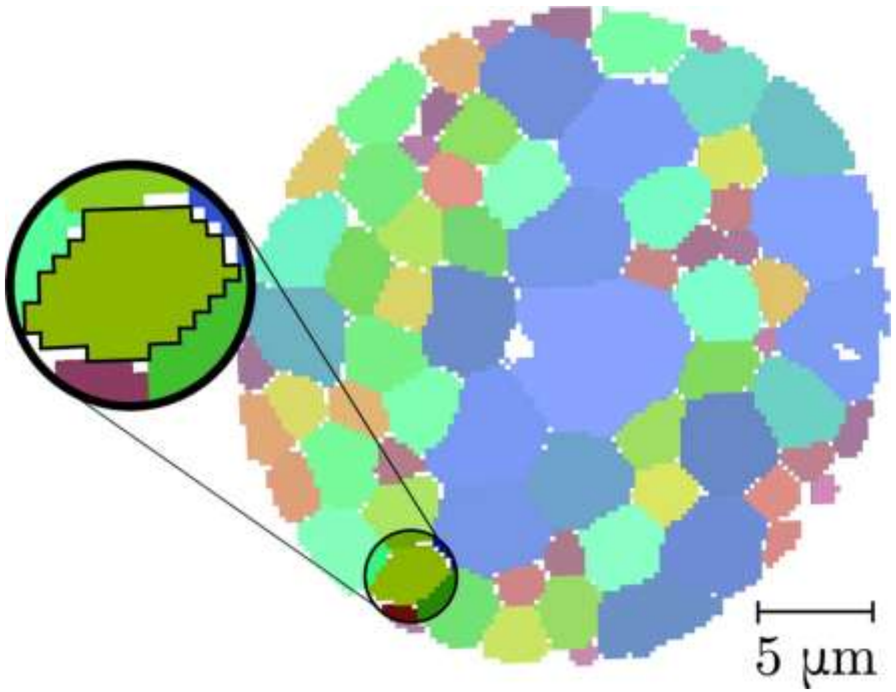

Orientation – does not shift peaks radially

Strain – shifts peaks in all directions

JAC JOURNAL OF APPLIED CRYSTALLOGRAPHY
ISSN 1600-5767

Reconstructing intragranular strain fields in polycrystalline materials from scanning 3DXRD data

N. Axel Henningsson,[a*] Stephen A. Hall,[a] Jonathan P. Wright[b] and Johan Hektor[c,d]

Volume 53 | Part 2 | April 2020 | Pages 314–325 | 10.11107/S1600576720001016

SCR = Single Crystal Refinement (+ Hayashi *et al*)
PCR = PolyCrystal Refinement
ASR = Algebraic Strain Refinement (linear formulation)

Acta Cryst. (2023). A79, 542–549

An efficient system matrix factorization method for scanning diffraction based strain tensor tomography

FOUNDATIONS ADVANCES

Axel Henningsson* and Stephen A. Hall

Strain + Orientation with small deformations

Methods are advancing rapidly…
… but experiments can still keep up with processing

3DXRD methods : how fast ? Time per voxel or time per orientation?

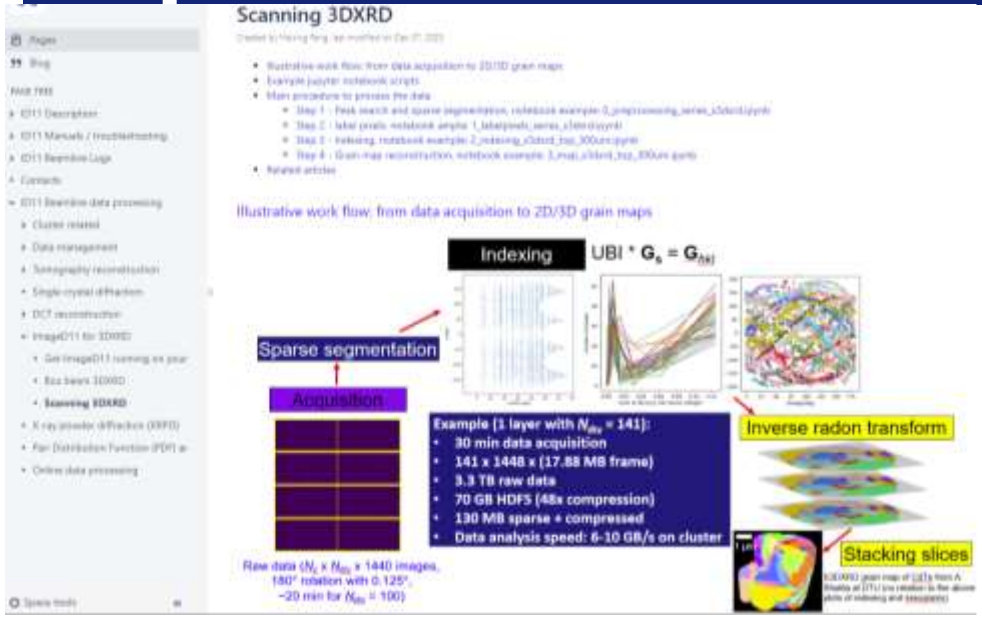

Scanning + Eiger

1 rotation ~ ≥12 s on nscope
30 steps : 6 minutes
30x30x30 volume = 3 hrs

100 steps = 20 minutes
1200 steps = 4 hours

In one shift:

3D : [49, 49, 49]
voxels=1e5

2D : [2400, 2400]
voxels=5.7e6

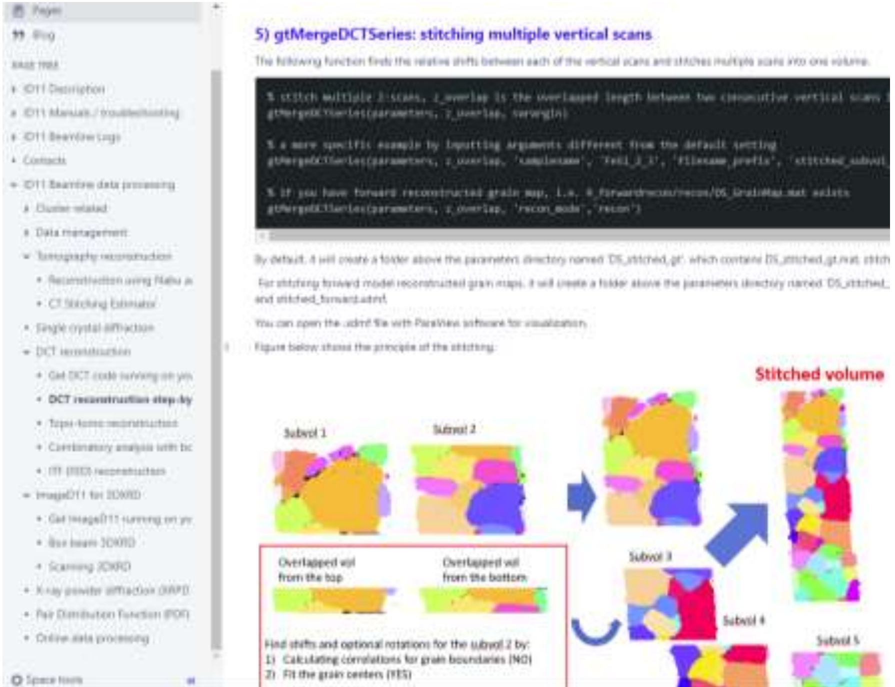

Near Field Detectors
~6 minutes per slice
(count longer for deformed)

Z-slices "HEDM":
~ [500, 500, 80]
voxels=2e7

nf-HEDM ~ 500x500x1

DCT ~ 500x500x400

Z-stack DCT volumes:
~ [500, 500, 400, 10] x 8
voxels=8e9
$3e^5$ orientations for 30^3

Haixing Fang has written docs! see: confluence.esrf.fr

Grain growth via DCT

Three-dimensional grain growth in pure iron. Part I. statistics on the grain level

Jin Zhang [a], Yubin Zhang [b,*], Wolfgang Ludwig [c], David Rowenhorst [d], Peter W. Voorhees [e], Henning F. Poulsen [a,**]

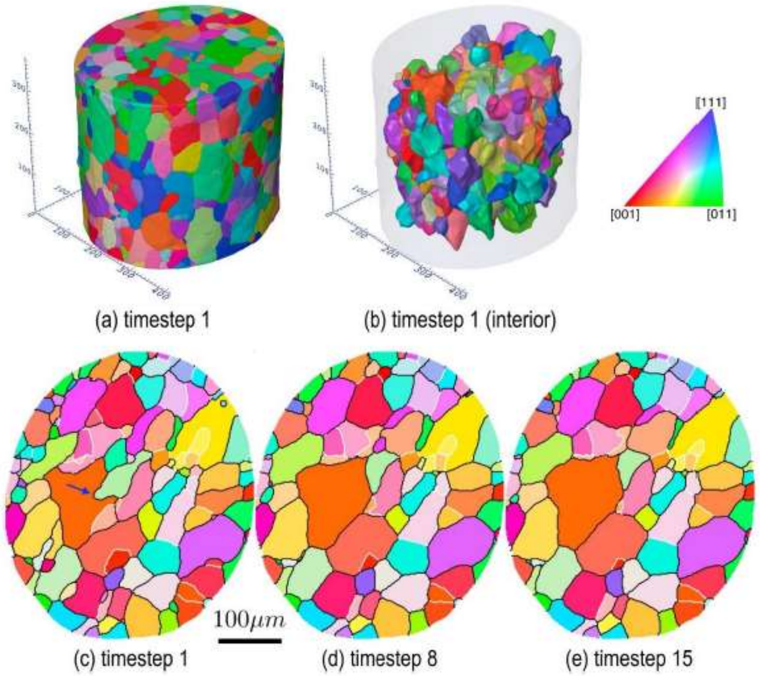

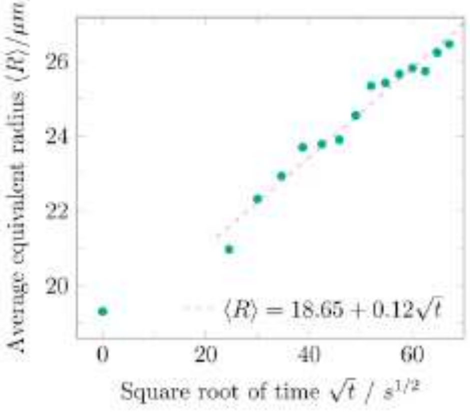

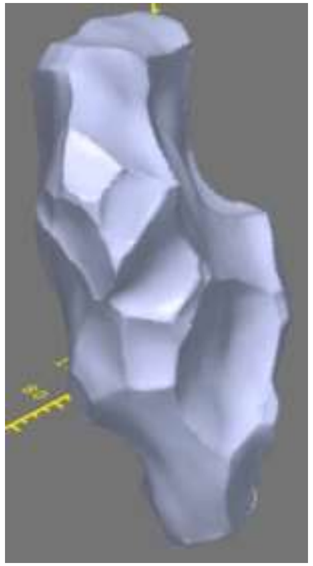

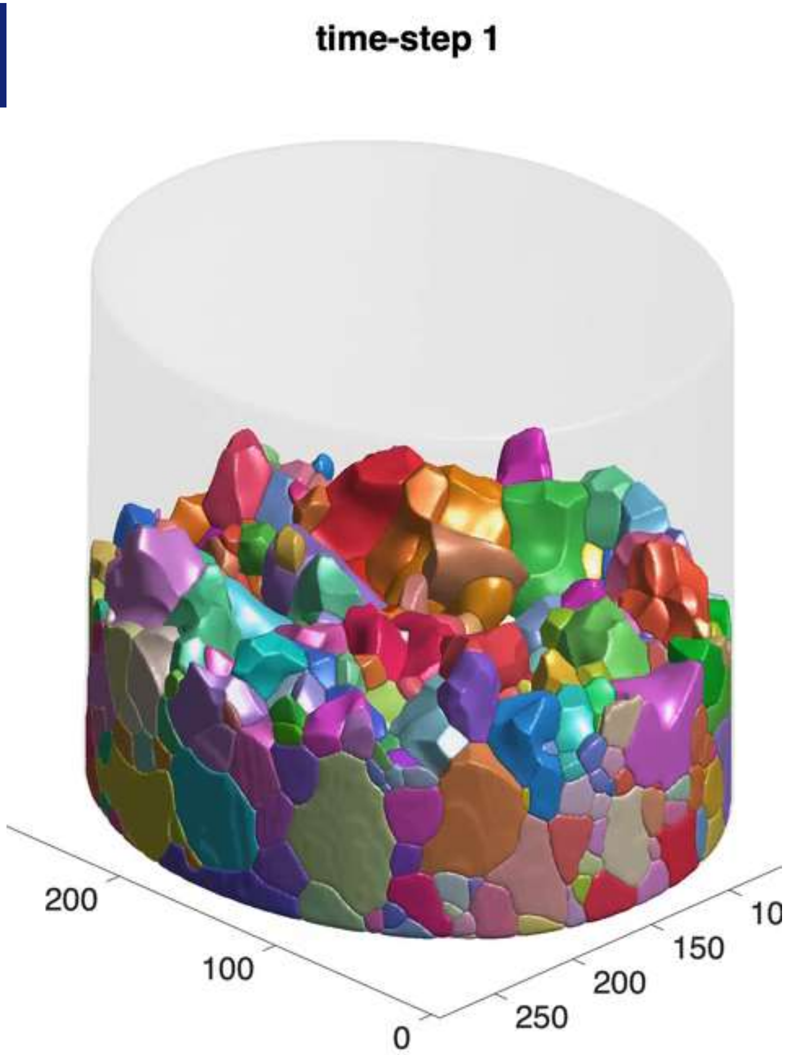

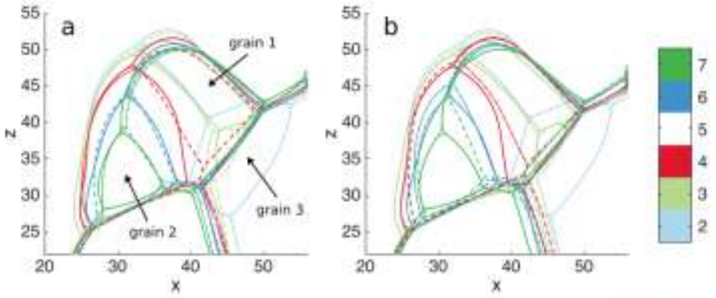

Fig. 9. Comparison between experiment (solid lines) and two types of simulations (dashed lines) for the topological change depicted in Fig. 8. (a) Simulations at time-step t_{8} with the resulting optimized reduced mobilities from local fittings in Table 2. (b) A two-step model running from time-step 2 to time-step 7. In both cases, time-step 5 is omitted due to a relatively larger uncertainty on the experimental data. The unit of axes is voxel size. Contours in the 2D section for various time-steps are identified by the bar to the right.

Grain boundary mobilities in polycrystals

Jin Zhang [a,b], Wolfgang Ludwig [c], Yubin Zhang [d], Hans Henrik B. Sørensen [e], David J. Rowenhorst [f], Akinori Yamanaka [g], Peter W. Voorhees [a], Henning F. Poulsen [*,b]

Acta Materialia 191 (2020) 211–220

Thank you

Haixing Fang

Wolfgang Ludwig

Pierre-Olivier Autran

James Ball

Pedro Damas-Resende

Zheheng Liu

Henri Gleyzolle

Eric Gagliardini

Emmanuel Papillon

Jose Maria Clement

STREAMLINE This project has received funding from the European Union's Horizon 2020 research and innovation programme under grant agreement No 870313. The European Synchrotron | ESRF